doi:10.14311/ppt.2024.1.17
Plasma Physics and Technology **11**(1):17–27, 2024

MODELLING OF GASIFICATION OF ORGANIC WASTE IN THERMAL-PLASMA CHEMICAL REACTORS

J. Jeništa[a,*], I. Hirka[b], O. Živný[a]

[a] *Institute of Plasma Physics of the CAS, U Slovanky 2525/1a, 182 00 Praha 8, Czech Republic*
[b] *formerly with IPP*
[*] jenista@ipp.cas.cz

Abstract. The paper presents the latest numerical simulations of gasification of wood particles and sewage sludge in two different thermal-plasma chemical reactors using either a unique DC-plasma torch stabilized by argon and water vortex or DC-plasma air torches. Numerical results of gasification and syngas production from crushed wood show that high syngas content (∼90%) was achieved for all studied currents (400–600 A) and wood particle diameters (0.2 mm – 20 mm). The CO and H_2 molar fractions for three different particle diameters for 400 A obtained by modelling at the exhaust outlet are in reasonably good agreement with the experimental values (CO–0.6, H_2–0.3). The gasification of sewage sludge by air plasma torches generate syngas of a lower quality (∼42%) due to a high nitrogen content in air.

Keywords: feeding rate, gasification, plasma torch, sewage sludge.

1. Introduction

The use of thermal plasma to gasify organic materials such as biomass and industrial wastes to produce synthesis gas is a promising way to harness surplus electricity from renewable sources. In the last two decades, extensive experimental research and numerical modelling of the gasification process has been carried out at the Institute of Plasma Physics of the CAS in Prague (hereafter IPP).

The scheme of a plasma-assisted gasification is shown in Figure 1. Organic material is supplied into the plasma stream having a high temperature and causing its partial volatilization. Using a plasma gas, having generally a different composition, and additional oxidizing medium for complete decomposition of volatilized species, a synthetic gas (syngas) is produced through the gasification process with some additional components, as tar, oil, soot and combustible gas. Syngas is the key-intermediate in the production of renewable transportation fuels, chemicals and electricity.

As the main advantages of plasma-assisted gasification we can mention for example:

1. plasma process can be applied on any organic material;
2. the presence of high plasma temperature and easy control of their values;
3. high intensity of uv radiation in plasma, suitable for destruction of complex molecules;
4. highly reactive conditions and presence of radicals;
5. high rate of heat transfer to treated material.

All these conditions guarantee obtaining high quality syngas while reducing tar and soot production.

Models of physical and chemical processes of biomass/sludge gasification including kinetics and computational fluid dynamics (hereafter CFD) have been of extensively studied over recent years, for example, [1–6]. However, majority of the published models has been focused to describe fluidized beds systems. Processes in thermal plasma reactor with special emphasis to steam plasma mixing with CO_2 and gasification of biomass particles to produce syngas have been studied previously at IPP both experimentally [7–10] and through CFD modelling [11–13]. Results of the gasification of the sewage sludge in a reactor with two air burners have not yet been published.

The aim of this paper is to present results of numerical simulations of two different gasification processes in a plasma chemical reactor. Namely, crushed wood using a unique DC-plasma torch stabilized by argon and water vortex, and sewage sludge using another DC-plasma torch stabilized by air. These processes were studied experimentally in different reactors. The water-argon DC-plasma torch, used for wood gasification, offers the advantage of low plasma mass flow rate, high enthalpy and temperature allowing to achieve an optimal conversion ratio with respect to synthesis gas production compared to other types of plasma torches. The gasification of the sewage sludge was studied in a reactor with two air burners with controllable mass flow rate and additional oxygen nozzles for better synthesis gas conversion ratio.

The modelling of gasification of wood particles comes from the previous study [13] where gasification of the wood particles with the mean particles diameters of 0. 2, 2 and 20 mm was studies under the plasma torch current of 400 A (see Table 4 in [13]). Here we present brand new results for the extended

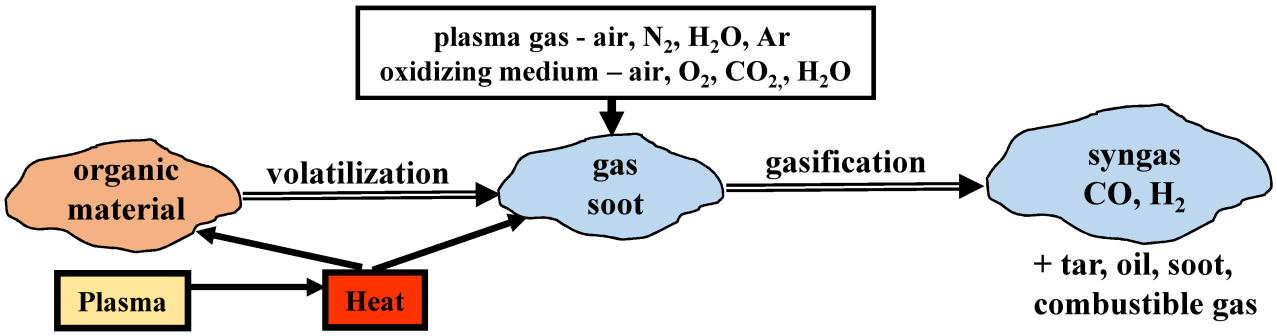

Figure 1. Principle of gasification process using a plasma source.

range of currents (400, 500 and 600 A) and mean particle diameters of 0.1, 0.2, 0.3, 0.5, 0.7, 1.0, 1.5, 2.0, 20 mm. The original results for 400 A [13] were recalculated with the new Ansys Fluent 2022 R1 [14] version.

The results presented in this study are original in terms of the physical-chemical model, the composition of the gasified material and the plasma torches used.

2. Physical-chemical model

2.1. Gasification of wood particles

The model description is given in detail in [13] so here we only briefly outline the main points.

Calculation of the gas phase includes the continuity, mass, energy and species transport conservation equations. Turbulence is calculated using the standard k-ε model. Diffusion flux of species takes laminar and turbulent flow regimes into account. Appropriate mass-weighted and volume-weighted mixing laws provide species mixing.

Trajectories of discrete phase particles follow from the momentum equation with the drag force, gravitational force, and thermophoretic force. The particle diameters are modelled by Rosin-Rammler distribution [15] with the idealized mean spherical particle diameters between 0.1 and 20 mm and the exponential factor equal to 3.5. The solid particles enter the region in the reactor heated up by a plasma jet. Heat transfer from plasma towards wood particles causes their heating, evaporation and boiling, creating thus a gaseous phase called 'wood volatiles'. It is assumed that each particle has a capacity of complete volatilization without unburnt fraction (soot or ash), in that case volatile component fraction is one. The wood volatiles arisen enter into chemical reactions forming syngas.

The empirical formula $C_{1.69}H_{2.37}O_{(g)}$ represents one monomer of gasified wood produced in our experiments in a plasma reactor as determined experimentally by elemental analysis. The adopted overall reaction scheme of syngas production from volatilized wood consists of two simultaneous irreversible reactions

$$C_{1.69}H_{2.37}O + 0.69\,CO_2 \rightarrow 2.38\,CO + 1.185\,H_2, \quad (1)$$

$$C_{1.69}H_{2.37}O + 0.121\,H_2O + 0.569\,CO_2 \rightarrow \rightarrow 2.259\,CO + 1.306\,H_2. \quad (2)$$

The reaction kinetics model discern two limiting cases, namely laminar finite rate model where reaction rates are given by usual Arrhenius expressions and turbulent model where reaction rates are controlled by the turbulence.

The inner volume of the reaction chamber is 0.206 m^3. The chamber is equipped with water-argon plasma torch stabilized by water swirl and axial argon gas flow. Calculations were carried out for 400, 500, 600 A. The corresponding mean water-argon plasma temperature and velocity at the outlet nozzle exit with the nozzle diameter of 6 mm, based on our former experiments [16], are 14,500 K and 2,635 m/s (400 A), 15,400 K and 3,247 m/s (500 A), and 16,200 K and 4,230 m/s (600 A). Steam plasma flow rates are 0.271 g/s (400 A), 0.285 g/s (500 A), 0.325 g/s (600 A). Injected gas flow consists of 98.75% CO_2 and 1.25% of N_2 with the flow rate 6.6 g/s. Feeding rate of crushed wood is 25 kg/h.

No slip conditions are applied for velocities at the reaction chamber walls. Heat flux in the range of 5–50 $Wm^{-2}K^{-1}$ were specified on different chamber walls to achieve thermal losses of 22 kW to the reactor walls and 8 kW to the anode based on the previous measurements at IPP.

The modification of the original code was made in Ansys Fluent 2022 R1 [14] program package. The discrete phase (i.e. wood particles) is modelled via Euler-Lagrangian discrete phase model. The discrete phase (that is dispersed into the viscous continuum) can exchange mass, momentum and energy with the continuum. The wood particle trajectories are computed individually every 5th iteration of the fluid phase. All runs were calculated as a stationary problem with 3000 iterations. The mesh consists totally of ~1,290,000 triangular and quadrilateral elements.

2.2. Gasification of sewage sludge

Model for the gasification of sewage sludge is the same in some aspects as the wood gasification model. Here we highlight only the main differences with regard to the previous model.

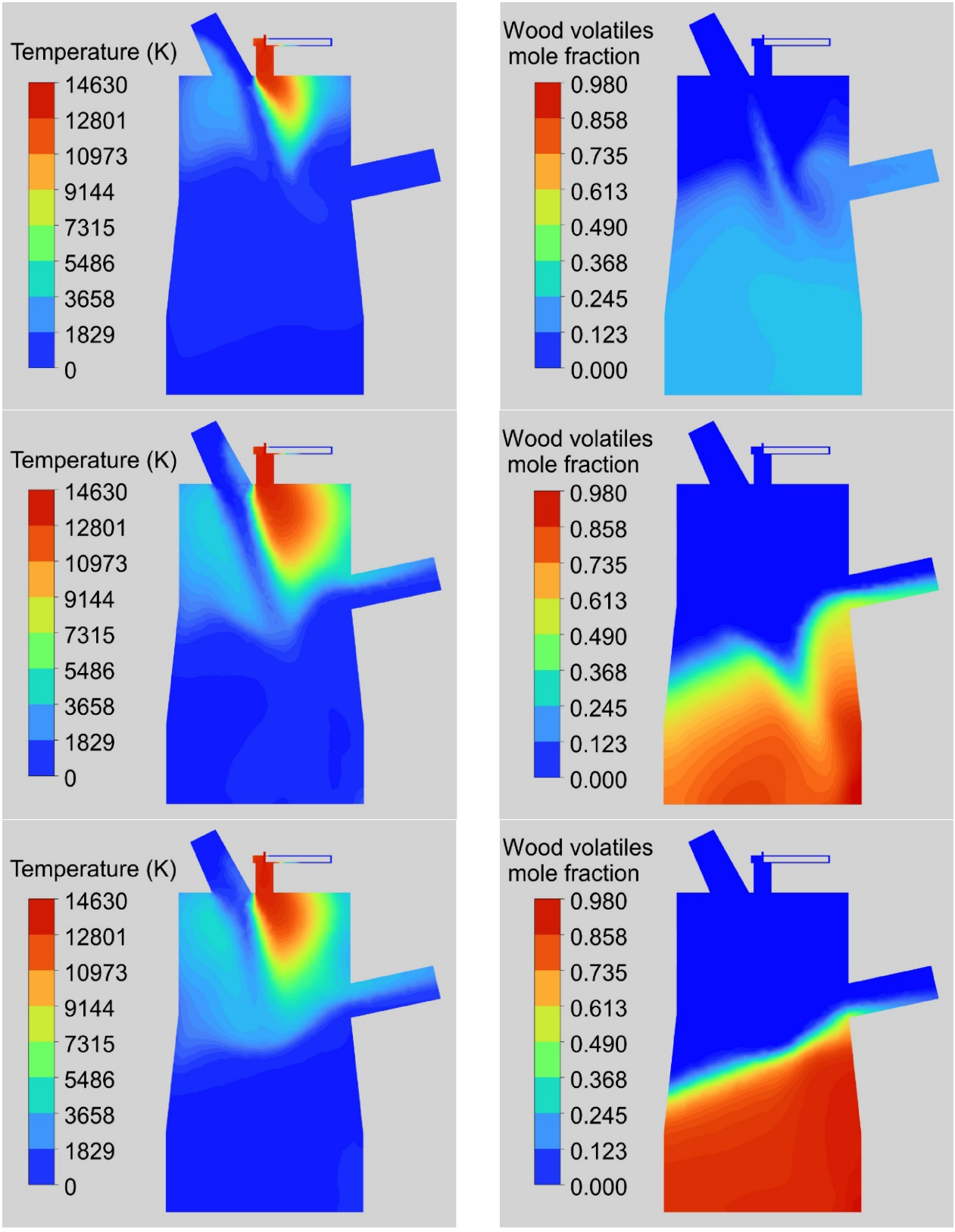

Figure 2. Temperature distribution (left) and mean wood volatiles mole fraction (right) in a chamber middle-cross-section for three different diameters of wood particles, 0.2 mm (top), 1 mm (middle), 20 mm (bottom) at 400 A.

Turbulence is calculated using the SST k-ω model (Shear-Stress Transport) [17]. Trajectories of discrete phase particles are additionally affected by the rotation of particles (a rotational drag law [18], Magnus lift force by Oesterle et al [19]), two-way turbulence coupling and turbulent dispersion calculated by discrete random walk model [20]. Since the sludge particles have the shape of a twisted cylinder, the shape factor

φ=0.7 was adopted to correct a fluid dynamic drag for a non-spherical shape [21]. The shape factor φ is the ratio of the surface area of a sphere having the same volume as the particle to the actual surface area of the particle. Its value cannot exceed 1, a value lower than 1 does not imply a lower fluid dynamic drag due to a complex dependence of a fluid dynamic drag on φ. A fluid dynamic drag for non-spherical particles is generally higher than for spherical ones. The main sludge particle diameter as modelled by Rosin-Rammler distribution is 8 mm with the exponential factor equal to 5 [15]. The volatile fraction of the particles, based on approximate estimate, is ∼63%, the unburnt fraction of sludge is deposited at the chamber bottom as slag.

Since we do not know the chemical composition of the mixture, but only the elemental composition, we cannot construct a reaction kinetic scenario. In this case, the chemical composition in the chamber is calculated from the equilibrium thermodynamic composition as a function of temperature.

Internal volume of the reaction chamber is 0.46 m^3. The chamber is equipped with two air plasma torches stabilized by axial flow. The diameter of the nozzles of both plasma torches is 15 mm. The upper plasma torch has an input power of 150 kW and a flow rate of 15 g/s, the lower one 85 kW with a flow rate of 10 g/s. The mean plasma temperature at the plasma torch nozzles is slightly below 6 kK.

Calculations were carried out for the sludge feeding rates of 50, 70, and 100 kg/h. Temperatures are applied as thermal boundary conditions on the reactor walls in the range of 800–1600 K based on experiments.

The code was developed in Ansys Fluent 2022 R1 [14] program package. The mesh is composed of totally ∼735,000 polyhedral elements. All calculations were running as a time-dependent problem. The sludge particle trajectories are computed individually every time iteration (lasting 1 second) of the fluid phase. Each calculation was completed after 600 iterations representing 10 minutes of a real time. Numerical tests have shown that this number of iterations is more than sufficient to achieve a stationary converged solution.

3. Numerical results

It should be pointed out that physical quantities fluctuate, as a result of fluid dynamic phenomena in the reaction chamber and interaction of particles with hot gas, after reaching steady state in both models. The graphs presented show the mean values of quantities over the entire iteration interval.

In the following plots (Figures 2–4) a middle-cross-section of the reactor for wood gasification is displayed. The plasma torch is mounted on the top, wooden particles with oxidizing agents are supplied by the inclined cone, and the exhaust pipe is on the right side.

It is obvious from the plots for 400 A (Figure 2) that the temperature is distributed non-uniformly within the whole volume of the reactor chamber. The highest temperatures are reached in the tube where the plasma flows into the chamber and in the adjacent area of the chamber, the higher temperatures are also deflected to the right due to the inflow of the injected particles and supporting gases. The maximum plasma temperature at the nozzle outlet is 14,630 K. The high temperature region in the upper right corner of the chamber increases with particle diameter and has the largest dimensions for a feed particle diameter around 1 mm. This tendency can be attributed to the larger effective surface of the smallest particles ($\leq$ 1 mm) and their more effective interaction with surrounding plasma flow and reacting gas.

Mole fractions of wood volatiles reveal much lower mole fractions for wood dust at the bottom of the chamber, and higher values for larger particles. This fact can be explained by an incomplete volatilization of larger particles in the upper parts of the chamber during their reaction with hot gas. The maximum values at the chamber bottom reach 0.24 for wood dust (0.2 mm) and 0.98 for 20 mm particles.

The computed distributions of CO mole fractions (Figure 3 left) show a principal difference between the gasification of wood dust and larger particles. CO mole fraction for wood dust is distributed more uniformly in the reactor than in the case of larger particles. In addition, the mole fraction of species is higher in the upper part of the chamber for wood dust. This trend is caused by worsened mixing of reacting gases and wood volatiles with plasma flow for the case of larger particles due to longer volatilization time. The mean mole fraction of CO for wood dust at the exhaust pipe cross section is ∼0.48, for the larger particles ∼0.45. Even though the chemical reactions occur only in the thin layer, the reaction rate is considerably higher than macroscopic flow which still results to the high reaction yield. The distribution of hydrogen (Figure 3 right) reveals similar behavior as for CO, but with generally lower absolute values of the mean hydrogen mole fractions (∼0.24) at the exhaust pipe cross section.

Comparison of CO and H_2 mole fractions with experiments [7] shows a reasonable agreement. Experiments have been carried out for a broader range of torch powers (95 - 152 kW), particle feed rates (6.9 - 47 kg/h) and a mixture of wood sawdust particle diameters (0.2 mm up to several mm). On the other hand, well-defined sawdust particle diameters (0.2, 0.5, 1, 2 mm) with prescribed size distributions were used in the calculations. The final evaluated experimental mole fractions of CO and H_2 for a sawdust mixture are 0.6 and 0.3 respectively at the pressure outlet (i.e., at the end of the outlet pipe) under the 400 A torch current. The calculated maximum values of CO mole fraction at the end of the outlet pipe are 0.48, 0.56 and 0.53 (for 400 A and particle diameters of 0.2, 1,

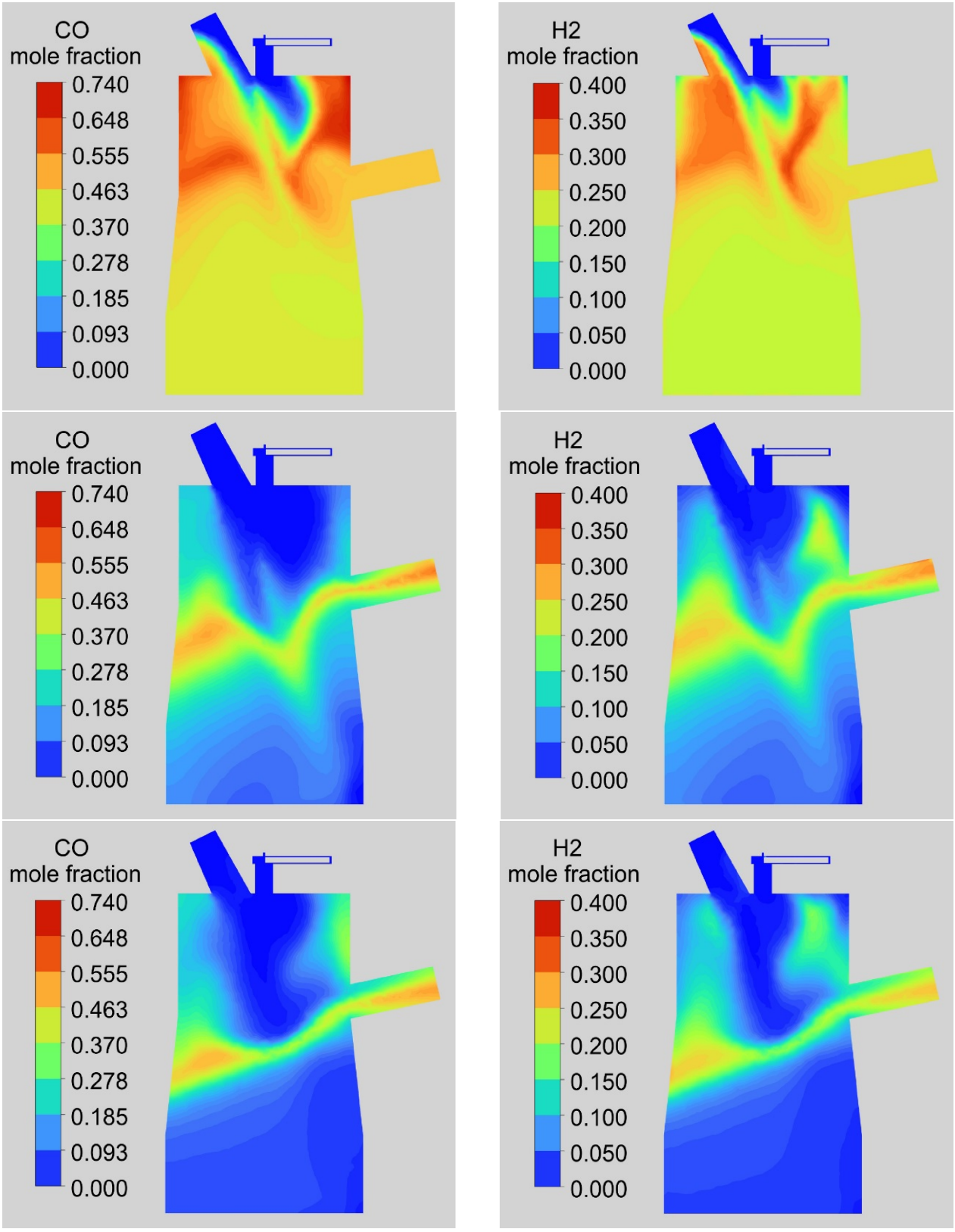

Figure 3. Mean mole fractions of CO (left) and H_2 (right) in a chamber middle-cross-section for three different diameters of wood particles, 0.2 mm (top), 1 mm (middle), 20 mm (bottom) at 400 A.

2 mm respectively); the mean values over the pressure outlet area are 0.48, 0.48, and 0.46. Similarly, the calculated maximum values of H_2 mole fraction are 0.25, 0.29 and 0.26 with the mean values of 0.24, 0.25, and 0.24. The agreement of the calculation with the experiment is reasonable, when we realize that the set of diameters of wooden particles in the experiment does not exactly match the simulation, and also the

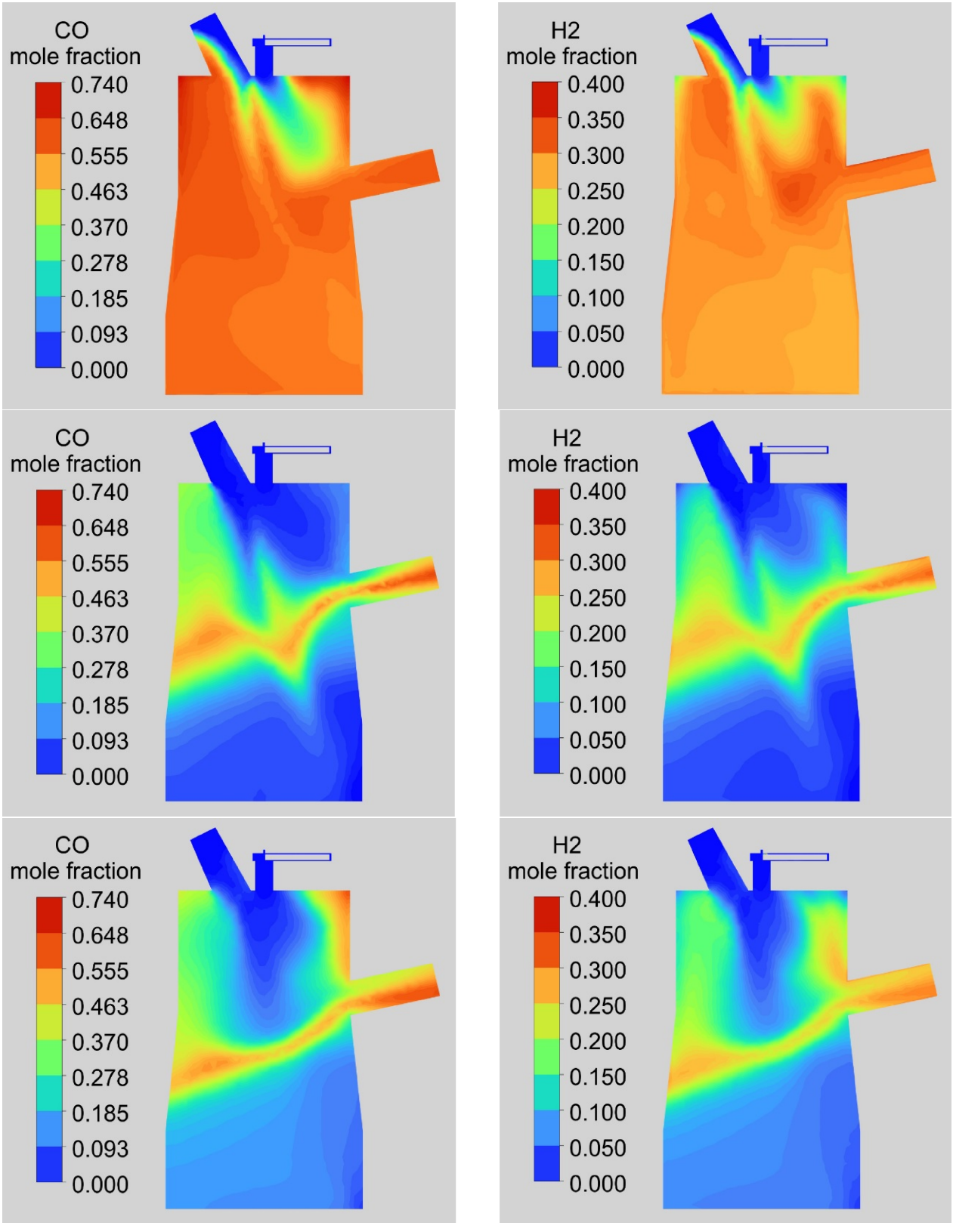

Figure 4. Mole fractions of CO (left) and H_2 (right) in a chamber middle-cross-section for three different diameters of wood particles, 0.2 mm (top), 1 mm (middle), 20 mm (bottom) at 600 A.

operating parameters of the plasma torch as well as the particle feed rate differ slightly from the simulated conditions.

Figure 4 depicts also the CO and H_2 mole fractions in the chamber, but for an increased plasma torch power corresponding to 600 A. The contours of mole fractions are qualitatively similar to those for 400 A, only with higher values. The mean mole frac-

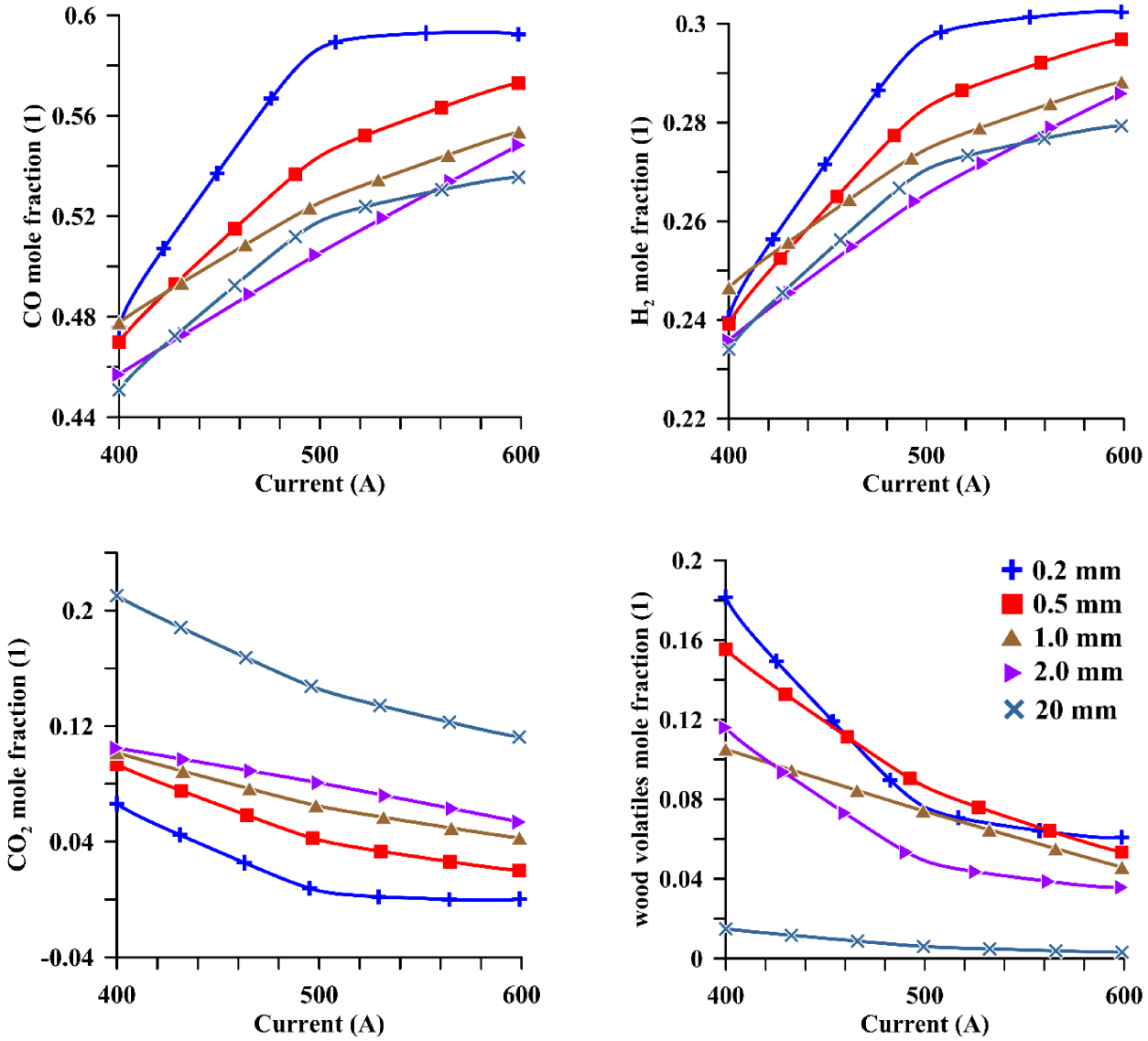

Figure 5. Mean mole fractions of CO (top left), H_2 (top right), CO_2 (bottom left) and wood volatiles (bottom right) across the exhaust pipe cross section as functions of current for different wood particle diameters.

tion of CO at the exhaust pipe cross section range between 0.59 (wood dust) and 0.53 (20 mm), for H_2 between 0.30 (wood dust) and 0.28 (20 mm). The results demonstrate that by increasing the power of the plasma torch, higher amounts of synthetic gas can be achieved in the gasification process.

Mean mole fractions of CO, H_2, CO_2 and wood volatiles at the exhaust pipe cross section as functions of current are illustrated in Figure 5. It is clear from the CO and H_2 mole fractions that higher values are obtained for higher currents and for small wood particle diameters. The amount of the additive gas CO_2 decreases with current and increases with the wood particle diameter. This is a consequence of the higher CO and H_2 yield at the outlet for smaller particle diameters. The amount of wood volatiles also decreases with current. In the case of 20 mm particles the amount of wood volatiles is negligible because volatilization takes place mainly in the lower part of the chamber.

The results for gasification of sewage sludge are shown in the following Figures 6–9. Again, a middle-cross-section of the reactor is displayed. The plasma torch is mounted on the top (the second plasma torch at the reactor bottom, placed in a different plane, is shown only in Figure 6), sludge particles are supplied by a tube at the top, the exhaust tube for gas products is on the left side, the tube for a slag waste is on the bottom right.

Figure 6 shows temperature distribution in the middle-cross-section of the reactor (left) as well as in the plane of the bottom plasma torch (right) for 100 kg/h. The maximum plasma temperature in the plasma torch nozzles is 5900 K. The temperature of the plasma jet decreases rapidly with increasing distance from the nozzles. The temperature in the reaction chamber, except for the plasma stream where the temperature exceeds 2000 K, is in the range 1350-1800 K,

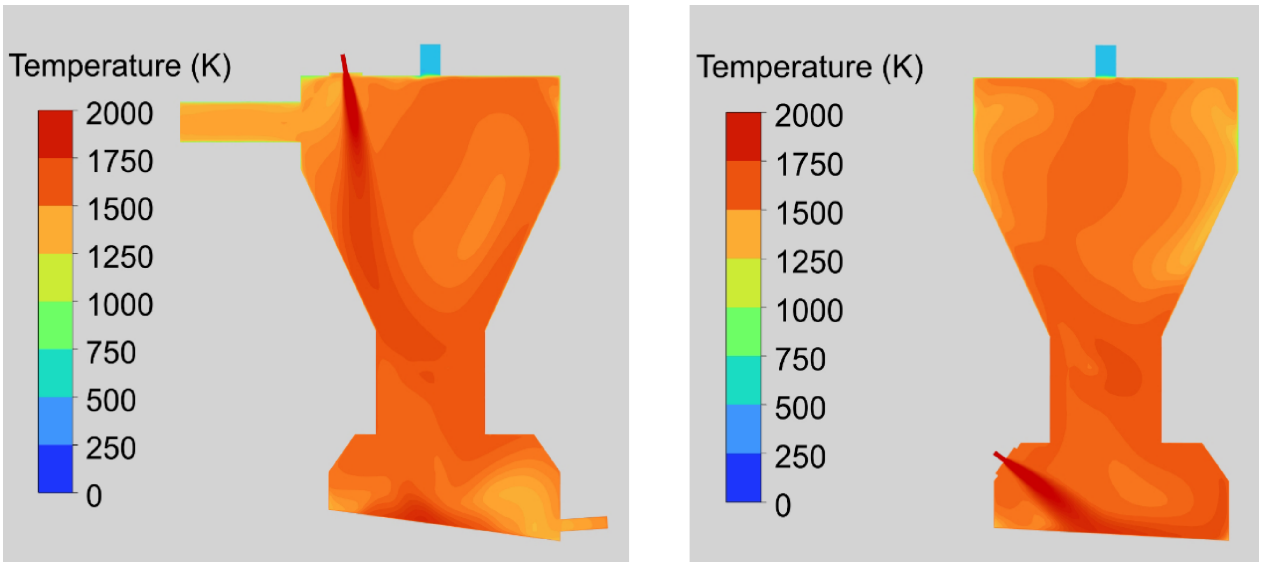

Figure 6. Temperature distribution in the top-plasma-torch (left) and bottom-plasma-torch (right) planes for the feeding rate of 100 kg/h.

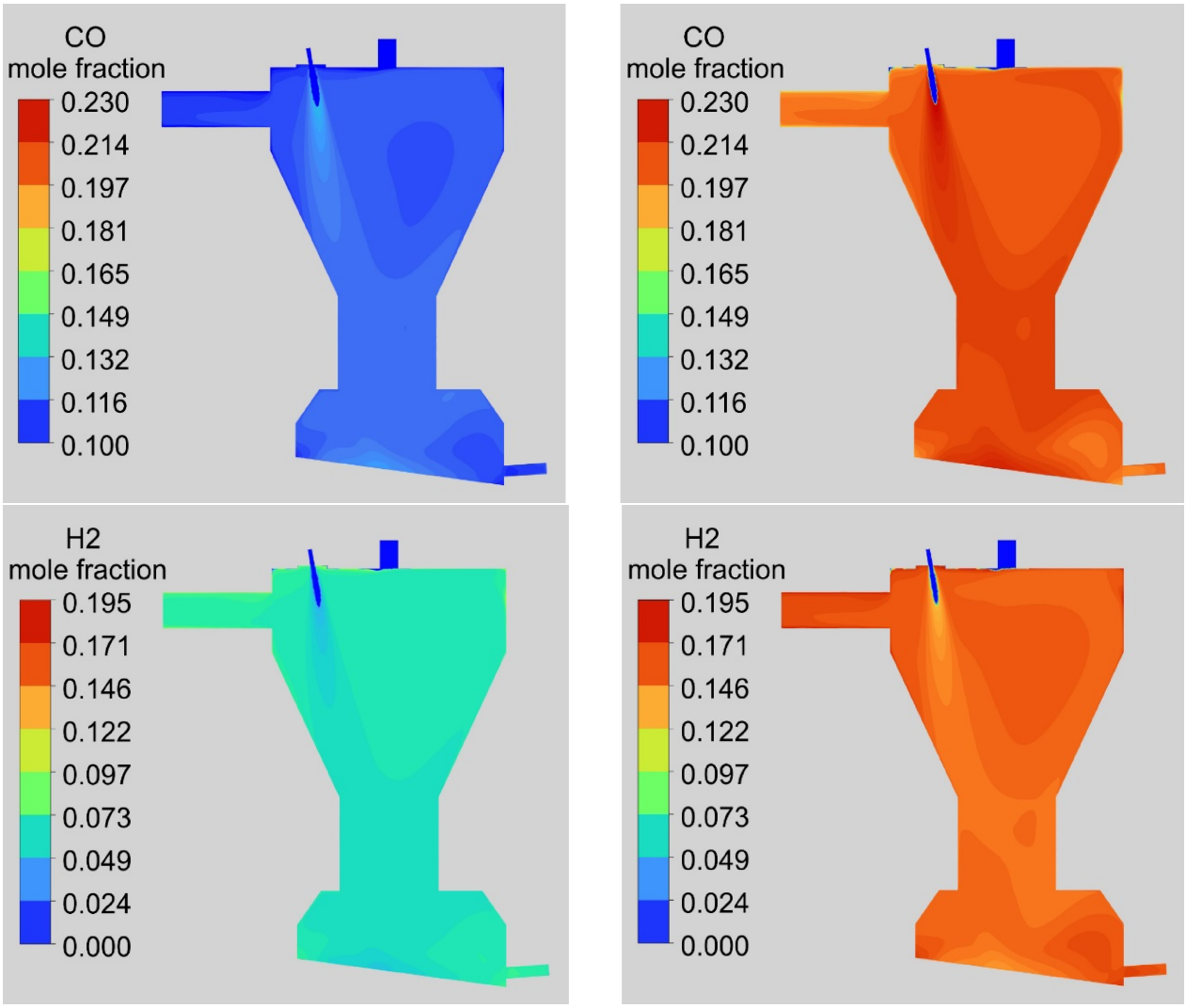

Figure 7. Mean CO (top) and H_2 (bottom) mole fractions for the feeding rates of 70 kg/h (left) and 100 kg/h (right).

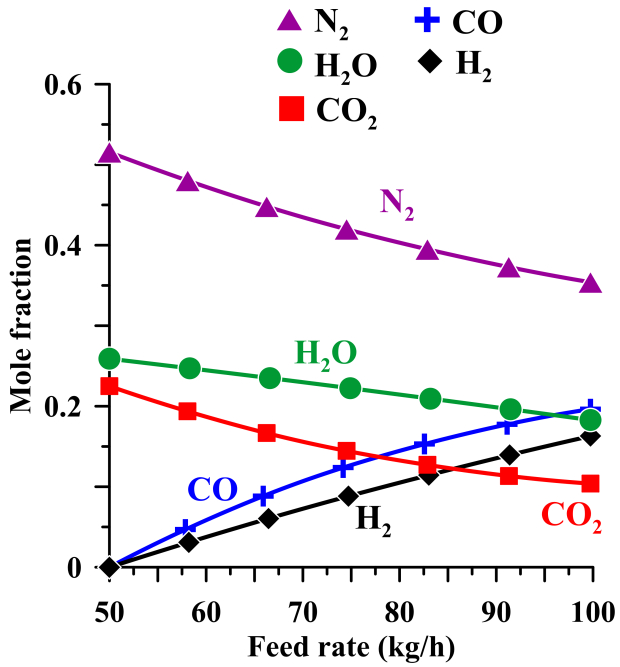

Figure 8. Mean mole fractions in dependence of the sludge feed rate.

the temperature in the exit tube is approximately 1400 K. For the lower particle feed rates (50-70 kg/h) the temperature field is qualitatively the same, only the temperatures are higher by about 100 K, with the exit tube temperature of about 1500 K.

Figure 7 displays mole fractions of CO and H_2 for 70 kg/h and 100 kg/h of the transported sludge particles into the chamber. The mole fractions increase with the feeding rate from ∼0.10 (70 kg/h) to ∼0.23 (100 kg/h) for CO and from ∼0.07 (70 kg/h) to ∼0.19 (100 kg/h) for H_2.

The mean mole fractions at the outlet pipe cross section in dependence of sludge feed rate shows Figure 8. The mole fraction of syngas (CO, H_2) increases, while the fraction of CO_2, H_2O and N_2 decreases with the feed rate. The amount of syngas is relatively small due to a high amount of nitrogen (35–52%) in a gas phase: CO = 11%, H_2 = 7% for 70 kg/h, and CO = 20%, H_2 = 16% for 100 kg/h. For 50 kg/h there is virtually no syngas in the mixture due to the large amount of oxygen fed into the chamber (totally 6 g/s of O_2).

The last Figure 9 displays the concentration of sludge particles at the chamber middle cross section. The maximum concentration in the plot is limited 10 kg/m^3. It should be mentioned that the term "dpm concentration" means the concentration of solid particles together with its liquid and vapor phases created in a gasification process (i.e., the total concentration of the particles in all phases in a cell). The higher feed rate case (100 kg/h – right picture) gives generally a higher concentration in the chamber volume compared to the lower feed one (50 kg/h – left picture). The highest concentration are found below the pipe that feeds the sludge into the chamber, in the constricted area with the oxygen flow into the chamber where strong mixing processes take place, and at the bottom of the chamber where ungasified particles deposit. Sludge particles also enter the hot gas region heated by the plasma torch due to the flow inside the chamber, which deflects the particles falling into the chamber away from the vertical direction.

4. Conclusion

CFD studies of the gasification process of crushed wood and industrial sewage sludge have been carried out. Thermal-plasma sources with a unique DC-plasma torch stabilized by axial argon flow and water vortex, and two DC-plasma air torches have been used in the present simulations. Numerical models have been developed or elaborated in Ansys Fluent [14]. The models are fully three-dimensional employing Euler-Lagrange approach for the calculation of the gas and solid phases, including description of physical and chemical processes in thermal plasma flow, interaction of injected particles with plasma, and chemical scenario for the generation of syngas. A model substance of crushed wood is represented by spherical wood particles with the mean diameters between 0.1 mm and 20 mm, for the sludge particles 8 mm.

It was confirmed that gasification of small wood particles (tenths of millimetres) gives a more homogeneous distribution of syngas in the reaction chamber volume than in the case of larger particles where the syngas is concentrated in the middle part of the reaction chamber. The amount of syngas in the volume and in the output tube increases with current and therefore with higher plasma torch power. Wood volatiles are concentrated in the lower part of the chamber and their amount increases with particle diameter. Calculated values of the CO and H_2 mole fractions for wood particle diameters 0.2, 1.0, and 20 mm (CO ∼0.46–0.48, H_2 ∼0.24–0.25) exhibit a reasonable agreement with available experiments (CO ∼0.6, H_2 ∼0.3) for 400 A.

The amount of generated syngas in the case of sludge gasification is relatively small (42% for 100 kg/h of feeding rate) compared to the crushed wood gasification. The reason is a high amount of nitrogen in air mixture but also the excessive amount of additive oxygen flowing to the reaction chamber (totally 6 g/s) causing practically no syngas appearance for 50 kg/h. Appropriate adaptation of operating conditions for maximum syngas yield is a matter for further parametric study. The highest concentration of the unburnt particles (corresponding approximately to slag) is at the bottom of the chamber and it increases with the feed rate.

The presented results clearly demonstrate the applicability of CFD models for calculations of flow, energy transfer, chemical constituents and waste gasification in reaction chambers. The existing numerical models

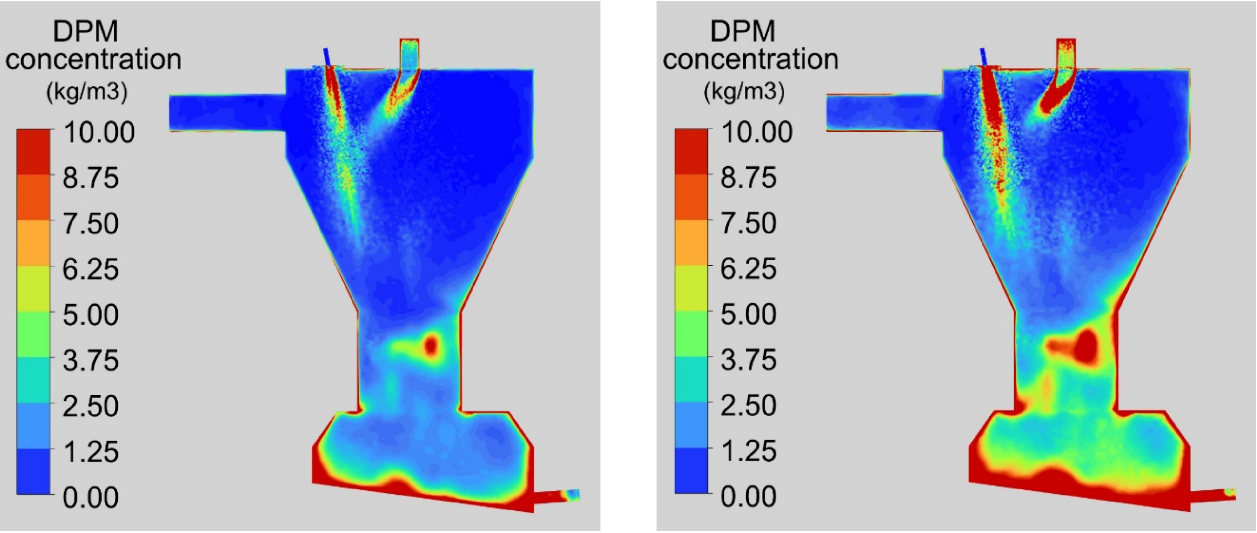

Figure 9. Concentration of solid ungasified particles together with its liquid and vapor phases in the chamber middle-cross-section. The higher feed rate 100 kg/h (right) provides a higher concentration in the chamber volume compared to the lower feed rate 50 kg/h (left).

can be further improved, e.g. by adjusting parameters in the turbulence models, modifying the particle gasification model and the chemical scenario.

Acknowledgements

Computational resources were provided by the e-INFRA CZ project (ID:90254), supported by the Ministry of Education, Youth and Sports of the Czech Republic.

References

[1] T. Y. Ahmed, M. M. Ahmad, S. Yusup, et al. Mathematical and computational approaches for design of biomass gasification for hydrogen production: A review. *Renewable and Sustainable Energy Reviews*, 16(4):2304–2315, 2012. doi:10.1016/j.rser.2012.01.035.

[2] R. I. Singh, A. Brink, and M. Hupa. CFD modeling to study fluidized bed combustion and gasification. *Applied Thermal Engineering*, 52(2):585–614, 2013. doi:10.1016/j.applthermaleng.2012.12.017.

[3] Q. Xue and R. Fox. Multi-fluid cfd modeling of biomass gasification in polydisperse fluidized-bed gasifiers. *Powder Technology*, 254:187–198, 2014. doi:10.1016/j.powtec.2014.01.025.

[4] S. Martínez-Lera and J. Pallarés Ranz. On the development of a polyolefin gasification modelling approach. *Fuel*, 197:518–527, 2017. doi:10.1016/j.fuel.2017.02.032.

[5] Werle and Sebastian. Impact of feedstock properties and operating conditions on sewage sludge gasification in a fixed bed gasifier. *Waste Management & Research*, 32(10):954–960, 2014. PMID: 24938298. doi:10.1177/0734242X14535654.

[6] P. Ziółkowski, J. Badur, H. Pawlak- Kruczek, et al. Mathematical modelling of gasification process of sewage sludge in reactor of negative CO_2 emission power plant. *Energy*, 244:122601, 2022. doi:10.1016/j.energy.2021.122601.

[7] M. Hrabovsky, M. Konrad, V. Kopecky, et al. Gasification of biomass in water/gas–stabilized plasma for syngas production. *Czech J Phys*, 56 (Suppl 2):B1199–B1206, 2006. doi:10.1007/s10582-006-0350-9.

[8] M. Hlina, M. Hrabovsky, T. Kavka, and M. Konrad. Production of high quality syngas from argon/water plasma gasification of biomass and waste. *Waste Management*, 34(1):63–66, 2014. doi:10.1016/j.wasman.2013.09.018.

[9] M. Hrabovsky, M. Konrad, V. Kopecky, et al. Pyrolysis of wood in arc plasma for syngas production. *High Temperature Material Processes: An International Quarterly of High-Technology Plasma Processes*, 10(4):557–570, 2006. doi:10.1615/HighTempMatProc.v10.i4.70.

[10] M. Hlína, M. Hrabovsky, V. Kopecký, et al. Plasma gasification of wood and production of gas with low content of tar. *Czechoslovak Journal of Physics*, 56:B1179–B1184, 2006. doi:10.1007/s10582-006-0347-4.

[11] S. Janssens. *Modeling of heat and mass transfer in a reactor for plasma gasification using a hybrid gas-water torch.* M.sc. thesis, Ghent University, Belgium, 2007.

[12] I. Hirka and M. Hrabovsky. Three-dimensional modeling of mixing of steam plasma jet with nitrogen in thermal plasma reactor. *High Temperature Material Processes: An International Quarterly of High-Technology Plasma Processes*, 14:1–9, 2009. doi:10.1615/HighTempMatProc.v14.i1-2.10.

[13] I. Hirka, O. Živný, and M. Hrabovsky. Numerical modelling of wood gasification in thermal plasma reactor. *Plasma Chemistry and Plasma Processing*, 37:947–965, 2017. doi:10.1007/s11090-017-9812-z.

[14] ANSYS FLUENT 2022 R1. URL: https://www.ansys.com.

[15] P. A. Vesilind. The Rosin-Rammler particle size distribution. *Resource Recovery and Conservation*, 5(3):275–277, 1980. doi:10.1016/0304-3967(80)90007-4.

[16] M. Hrabovsky. Water-stabilized plasma generators. *Pure and Applied Chemistry*, 70(6):1157–1162, 1998. doi:10.1351/pac199870061157.

[17] F. R. Menter. Two-equation eddy-viscosity turbulence models for engineering applications. *AIAA Journal*, 32(8):1598–1605, 1994. doi:10.2514/3.12149.

[18] S. C. R. Dennis, S. N. Singh, and D. B. Ingham. The steady flow due to a rotating sphere at low and moderate reynolds numbers. *J. Fluid Mech.*, 101:257–279, 1980. doi:10.1017/S0022112080001656.

[19] B. Oesterlé and T. Dinh. Experiments on the lift of a spinning sphere in a range of intermediate reynolds numbers. *Experiments in Fluids*, 25:16–22, 1998. doi:10.1007/s003480050203.

[20] A. D. Gosman and E. Ioannides. Aspects of computer simulation of liquid-fuelled combustors. *J. Energy*, 7(6):482–490, 1993. doi:10.2514/3.62687.

[21] A. Haider and O. Levenspiel. Drag coefficient and terminal velocity of spherical and nonspherical particles. *Powder Technology*, 58:63–70, 1989. doi:10.1016/0032-5910(89)80008-7.